Science Advances
AAAS

advances.sciencemag.org/cgi/content/full/6/42/eabb2459/DC1

Supplementary Materials for

A multimillennial climatic context for the megafaunal extinctions in Madagascar and Mascarene Islands

Hanying Li, Ashish Sinha*, Aurèle Anquetil André, Christoph Spötl, Hubert B. Vonhof, Arnaud Meunier, Gayatri Kathayat, Pengzhen Duan, Ny Riavo G. Voarintsoa, Youfeng Ning, Jayant Biswas, Peng Hu, Xianglei Li, Lijuan Sha, Jingyao Zhao, R. Lawrence Edwards, Hai Cheng*

*Corresponding author. Email: asinha@csudh.edu (A.S.); cheng021@xjtu.edu.cn (H.C.)

Published 16 October 2020, *Sci. Adv.* **6**, eabb2459 (2020)
DOI: 10.1126/sciadv.abb2459

The PDF file includes:

Figs. S1 to S10

Other Supplementary Material for this manuscript includes the following:

(available at advances.sciencemag.org/cgi/content/full/6/42/eabb2459/DC1)

Data files S1 and S2

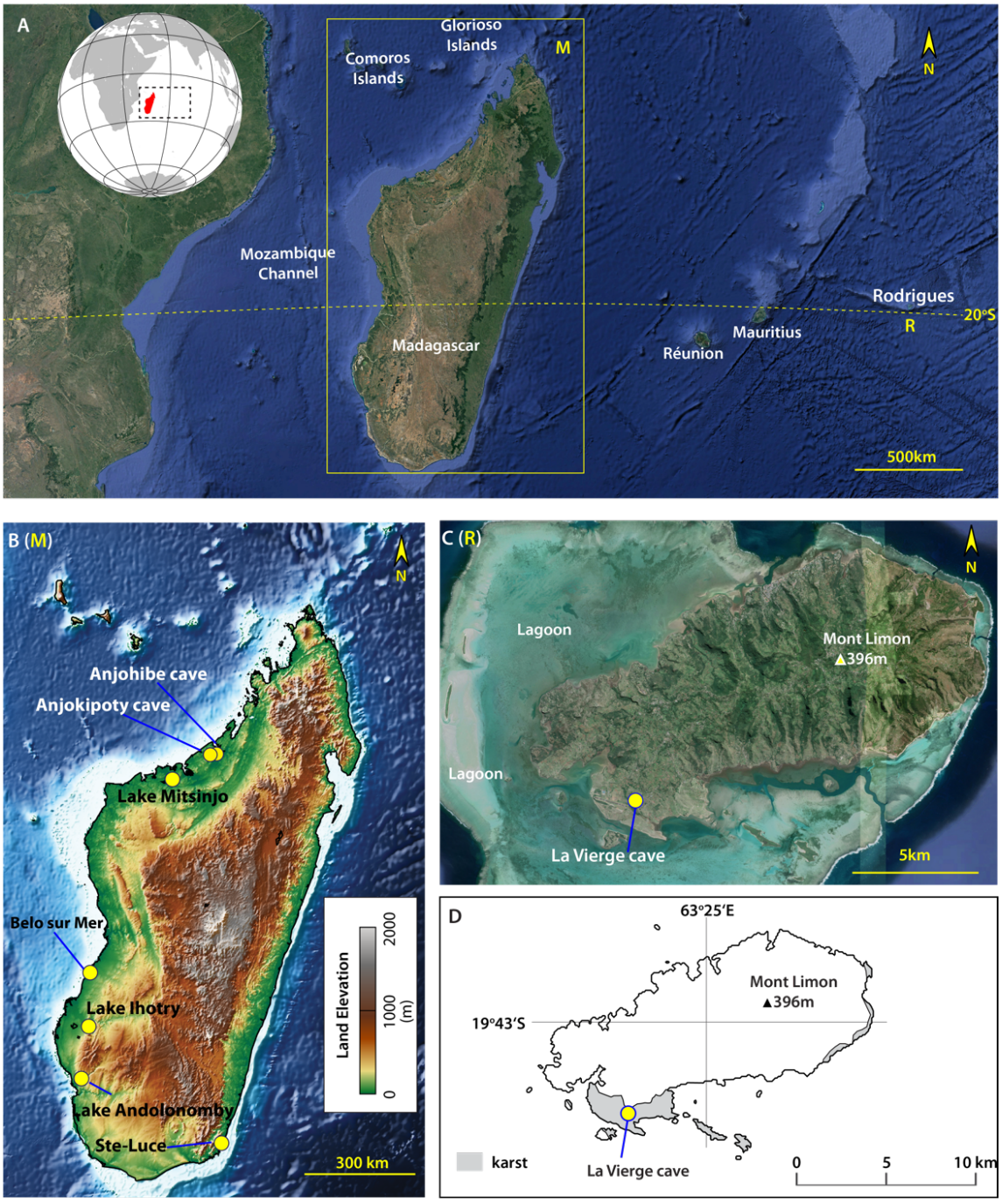

Fig. S1. Geographic context of the study area. (**A**) Google Earth image of the South West Indian Ocean region (dashed rectangle inside the inset) showing the islands of Madagascar and the Mascarenes (Réunion, Mauritius and Rodrigues). Areas marked by a yellow rectangle (M) and letter 'R' are shown in panels B and C, respectively. (**B**) The Digital Elevation Map (DEM) of Madagascar. Topography data are from NOAA's 1 arc minute ETOPO1 global grid (https://www.ngdc.noaa.gov/mgg/global/). Locations of Anjohibe cave (this study, *10, 26-29*), Anjokipoty cave (*28*), Lake Mitsinjo (*25*), Lake Ihotry (*20*), Lake Andolonomby (*23*), peatbog cores from Ste-Luce (*12*), and a subfossil sites at Belo sur Mer (*7*) are shown with yellow circles. (**C**) Google Earth image of the islands of Rodrigues and the surrounding lagoon. Locations of the La Vierge cave (this study) and Mont. Limon marking the highest land elevation (~396 m on the island are shown. (**D**) Outline map of Rodrigues showing the locations of La Vierge cave, karstified areas on the island (shaded), and Mont Limon.

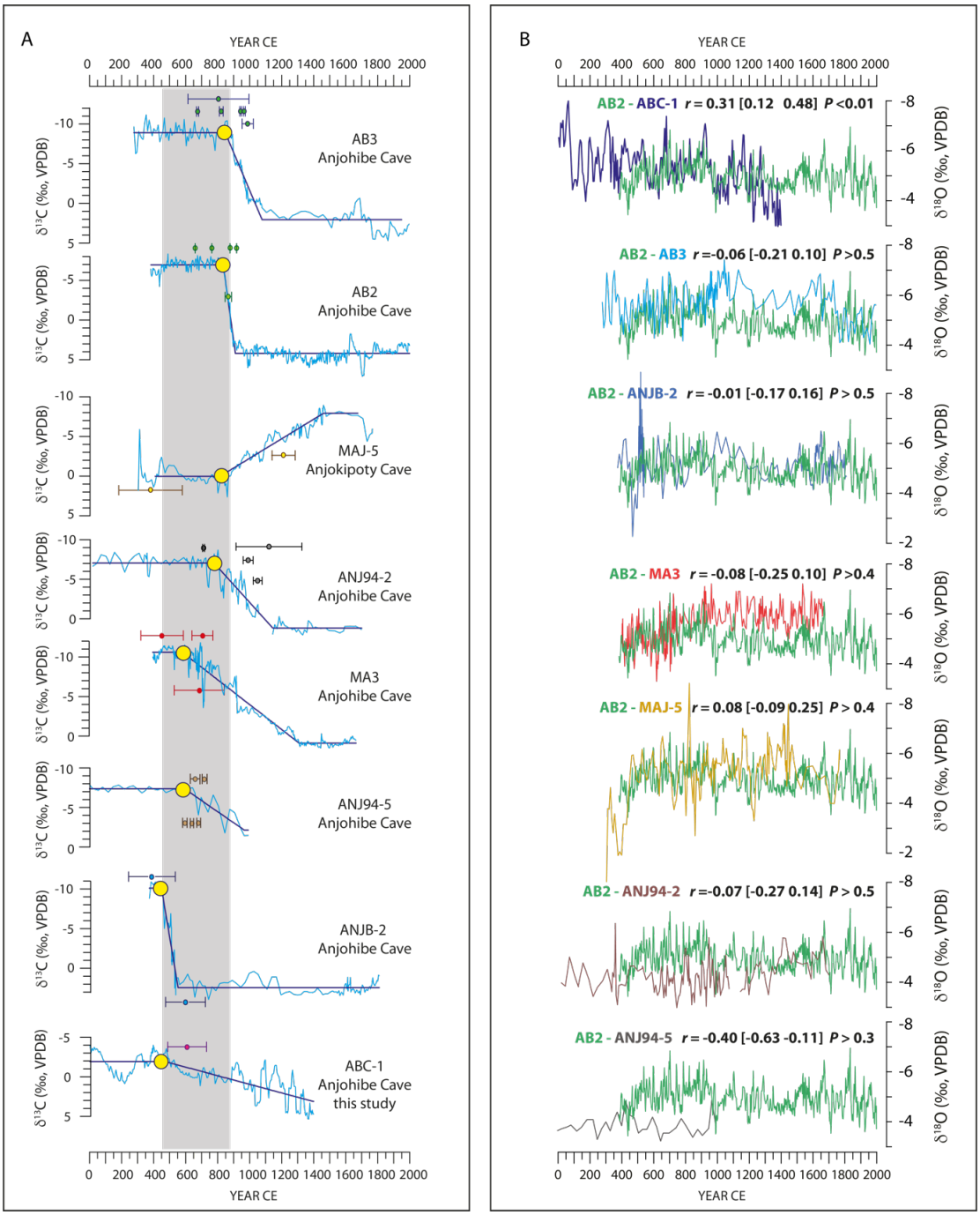

Fig.S2. Stacked comparisons of the Madagascar speleothem $\delta^{13}C$ and $\delta^{18}O$ records over the past 2000 years. (**A**) Published $\delta^{13}C$ records and ABC-1 (this study). The records from top to bottom are AB3 (*10*), AB2 (*26*), MAJ-5 (*28*), ANJ94-2 (*30*), MA3(*27*), ANJ94-5 (*29*), ANJB-2 (*28*) and ABC-1 (this study). All records are from Anjohibe cave except MAJ-5, which is from Anjokipoty cave. The 'change point' in each $\delta^{13}C$ profile (yellow dots) was identified using the RAMPFIT function (Materials and Methods). The quoted ^{230}Th dates and 2σ error bars around each change point are marked. Vertical grey bar represents the temporal range in the onset times of the positive $\delta^{13}C$ excursion. (**B**) Comparison between AB2 $\delta^{18}O$ record (*26*) with ABC-1 (this study) and other published $\delta^{18}O$ records from Madagascar. The correlation coefficients, 95% confidence intervals, and *P* values (after accounting for autocorrelation in each time series) are reported in each sub-panel. ABC-1, AB2, AB3, ANJB-2, MA3 and MAJ-5 time series were 10-year interpolated over the coeval periods. ANJ94-2 and ANJ94-5 were 15-year and 30-year interpolated, respectively.

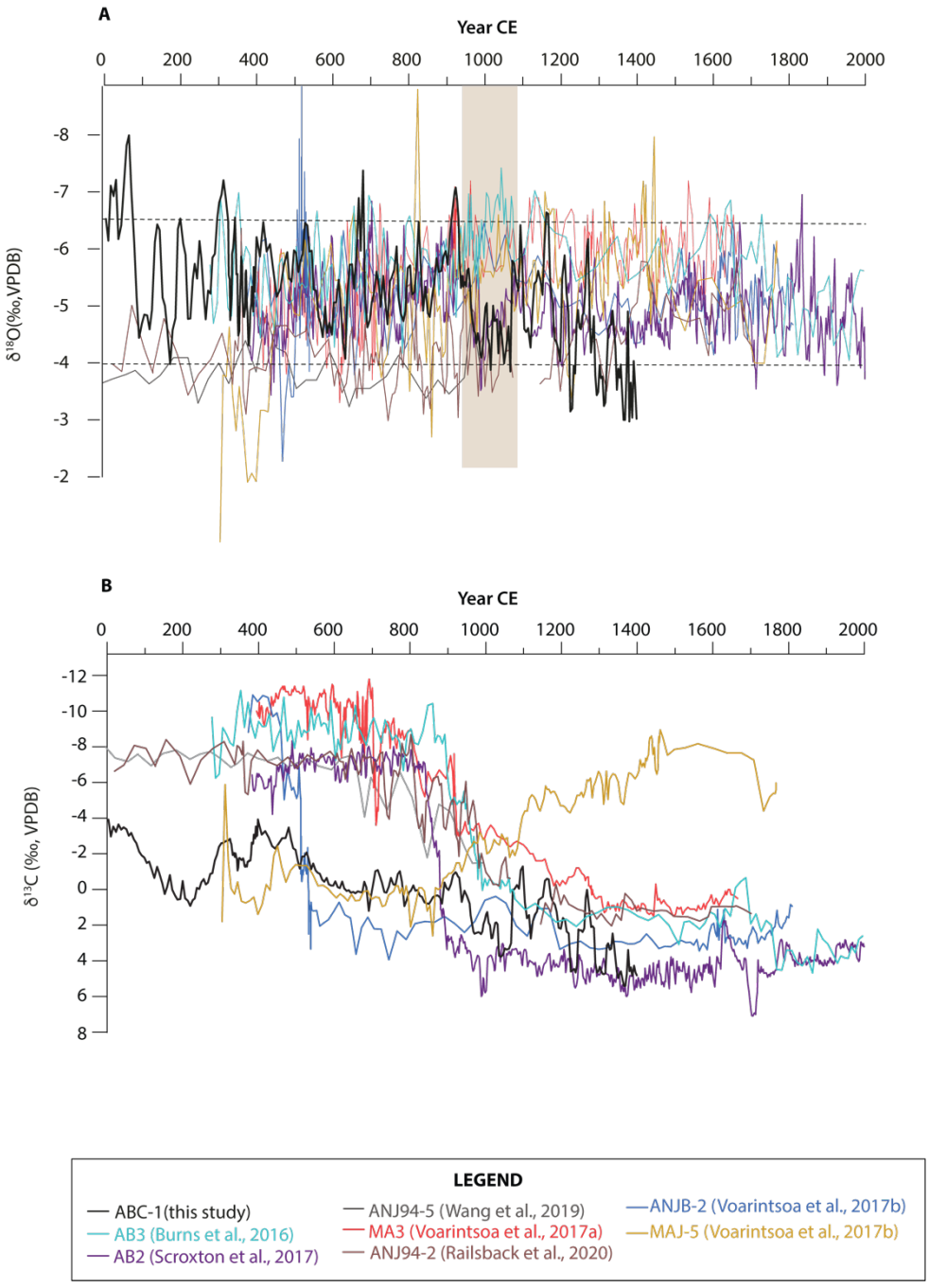

Fig.S3. Madagascar speleothem $\delta^{13}C$ and $\delta^{18}O$ records. (**A**) The $\delta^{18}O$ records of speleothem ABC-1 (this study, black) plotted together with other published speleothem $\delta^{18}O$ records from Madagascar (color coded by speleothem names) over the past 2000 years. About 90% of ABC-1 $\delta^{18}O$ values fall between -4 and -6.5 ‰ (dashed lines). The shaded bar (centered around 1000 CE) highlights a period of bi-modal distribution of $\delta^{18}O$ values. (**B**) the same as **A**, but for the $\delta^{13}C$ records.

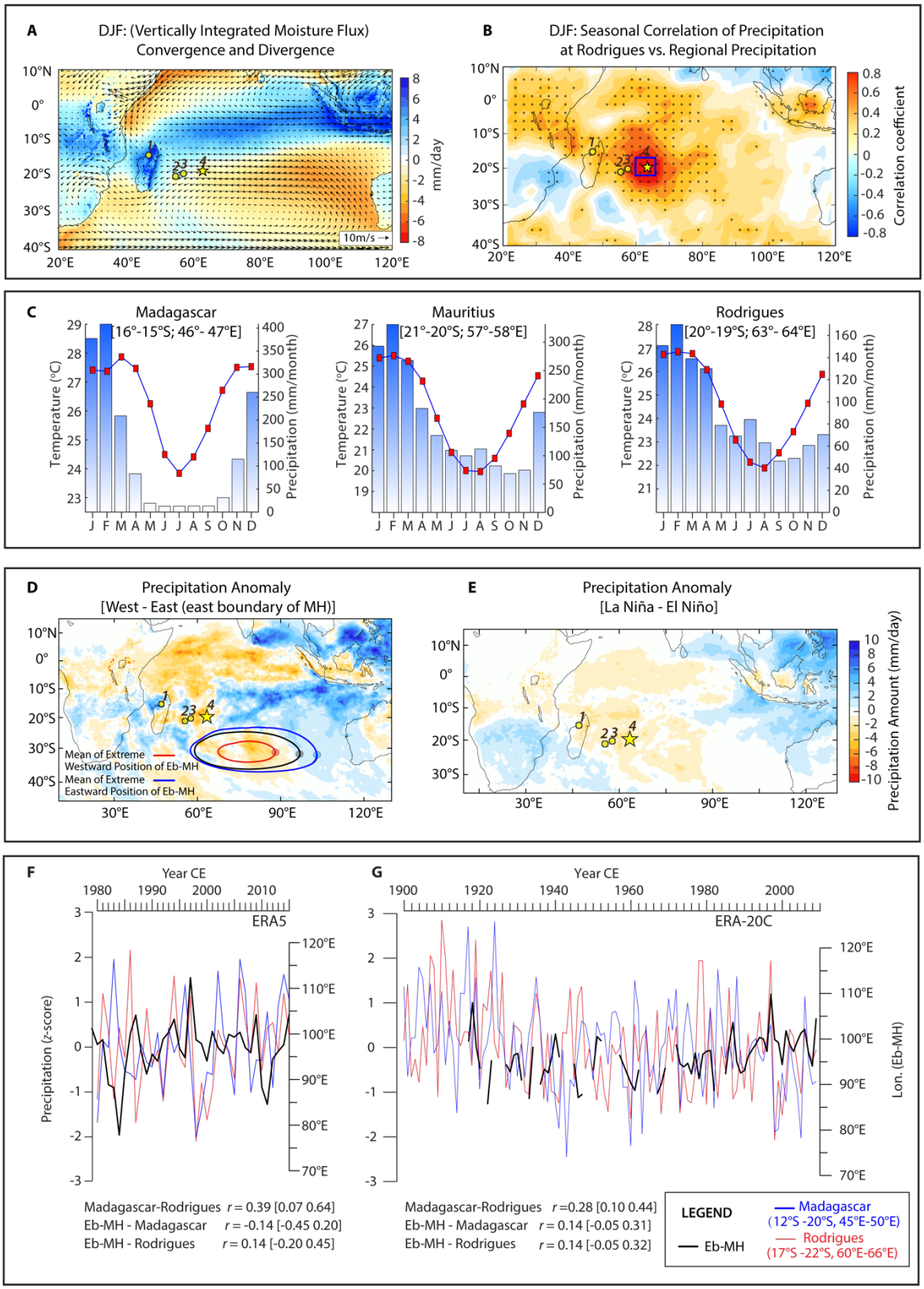

Fig.S4. Climate setting of Madagascar and the Mascarene Islands. (**A**) Climatology of near-surface (850 hPa) December-January-February (DJF) winds (arrows) and vertically integrated moisture flux and its convergence/divergence from the ERA5 dataset between 1980 and 2015. (**B**) Spatial correlation pattern between the DJF precipitation over Rodrigues (blue rectangle: 22°S -17°S, 60°E-66°E) and regional precipitation from GPCP v2.3 dataset between 1979 and 2015 (*60*). Stippling indicates significant

correlation ($P < 0.1$ level). (**C**) Climographs of precipitation (blue bars) and temperature (red squares connected with blue lines) at Madagascar (16°S -15°S, 46°E-47°E), Mauritius (21°S -20°S, 57°E-58°E) and Rodrigues (20°S -19°S, 63°E-64°E). High-resolution gridded data were obtained from Climatic Research Unit Time-Series version 4.03 (CRU TS4.03) (*59*). (**D**) Spatial patterns of DJF precipitation anomalies (ERA5) for years of anomalous westward (1984, 2011, 1983, 2010, 1982, 1985, 1989, 1991, 2000) and eastward (1997, 2015, 2009, 1987, 1994, 1979, 2001,2006, 1993) positions of the eastern boundary of the MH (Materials and Methods). Blue (red) line and dot are the mean of 9-year extreme eastward (westward) positions of the MH and its eastern boundary, respectively. Black line and dot are the mean of position of the MH and its eastern boundary for 1980 to 2015, respectively. (**E**) Spatial pattern of DJF precipitation anomalies (ERA5) for years marked by La Niña (1984, 1988, 1995, 1998, 1999, 2000, 2007, 2008, 2010, 2011) and El Niño (1979, 1987, 1991, 1994, 1997, 2002, 2004, 2006, 2009, 2014, 2015). Circles numbered from 1 to 3 and star (numbered 4) in **A, B, D** and **E** mark the locations of Madagascar, Réunion, Mauritius and Rodrigues, respectively. (**F**) Year-to-year comparisons (1980-2015) between the DJF eastern boundary of Mascarene High (Eb-MH) longitude position (black) with the ERA5 precipitation (*z*-score) for northern Madagascar [12°S -20°S, 45°E-50°E, (blue)] and Rodrigues [(17°S -22°S, 60°E-66°E (red line)] (Materials and Methods). (**G**) Same as **F** but for the period between 1900 and 2009 from ERA-20C data. The maximum of mean geopotential height at 850 hPa lower than 1535 gpm (the unit of geopotential height) during DJF leads to discontinuous Eb-MH time series. The correlation coefficient among three timeseries in each panel is listed below the **F** and **G**.

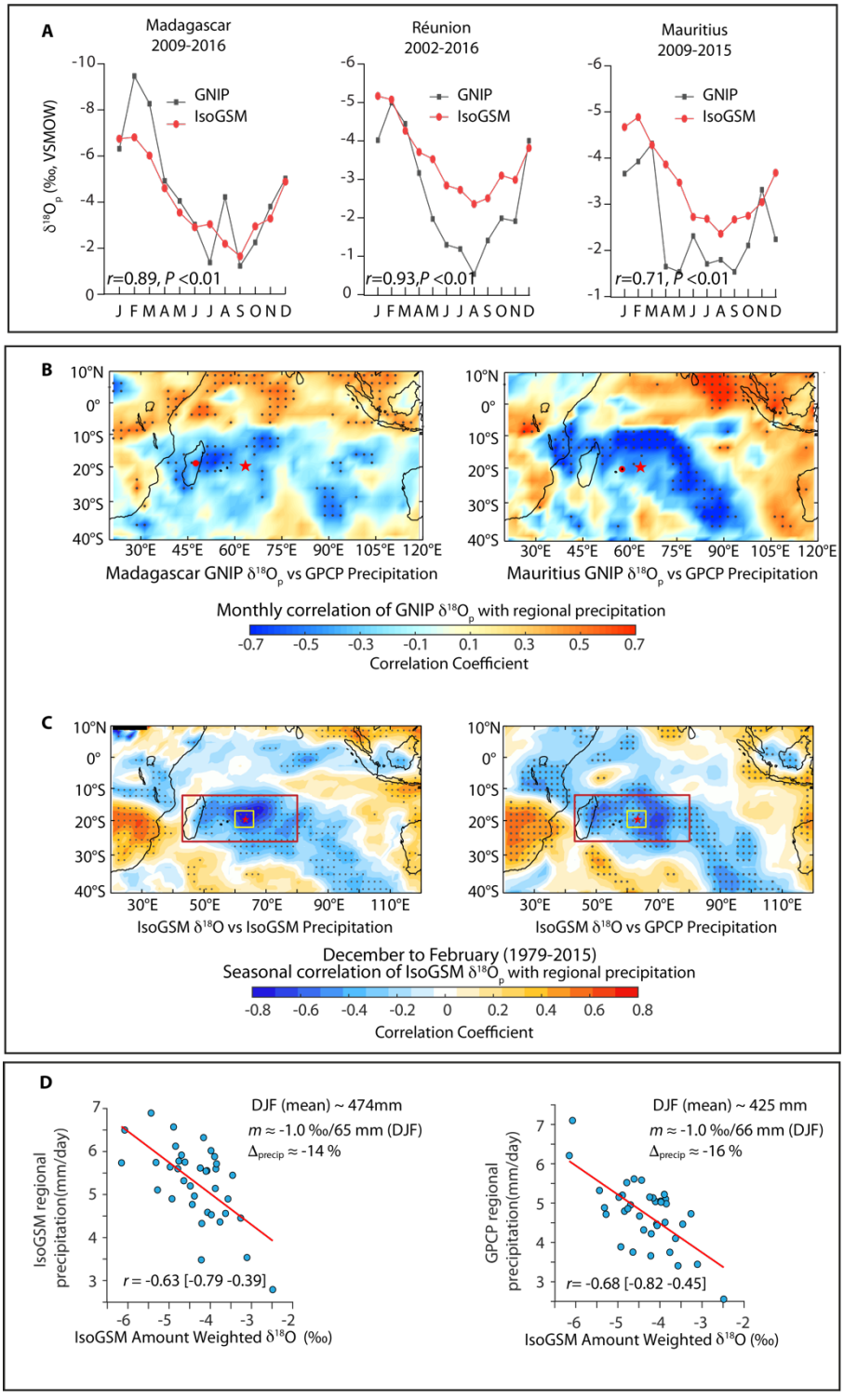

Fig. S5. Regional $\delta^{18}O_p$ data from GNIP and IsoGSM. **(A)** Comparisons of annual cycle in $\delta^{18}O_p$ from observed GNIP data (grey squares) and simulated data from IsoGSM (red squares) (*38*) at Antananarivo, Madagascar (18.9°S, 47.6°E, 1295 m a.s.l), Réunion (20.9°S, 55.5°E, 70 m a.s.l) and Mauritius (20.3°S, 57.5°E, 402 m a.s.l). The simulated $\delta^{18}O_p$ data were derived from the nearest gridded point of observation

sites (Materials and Methods). DJF spatial correlation between monthly GPCP precipitation and GNIP $\delta^{18}O_p$ from Madagascar (left panel) and Mauritius (right panel), respectively. The locations of Rodrigues and GNIP stations at Madagascar (star) and Mauritius (circle) are shown. (**C**) Spatial correlation between the DJF amount-weighted IsoGSM $\delta^{18}O_p$ averaged over the area around the Rodrigues (yellow rectangle) with the model-simulated rainfall amount (left panel) and GPCP precipitation (right panel) between 1979 and 2015. Stippling indicates significant correlation ($P < 0.1$). The locations of Rodrigues are marked by a star. (**D)** Correlation between the DJF amount-weighted $\delta^{18}O_p$ averaged over Rodrigues (yellow rectangles in panel **C**) versus simulated precipitation amount (left panel) and GPCP precipitation (right panel) averaged over an area marked by red rectangles in **C**. The mean precipitation amount over the region within red rectangle during DJF between 1979 and 2015 is ~ 474 mm (425 mm) in IsoGSM (GPCP) dataset. The slopes (m) of $\delta^{18}O_p$ and precipitation amount relationship yield a conversion of 1‰ increase in DJF $\delta^{18}O_p$ to ~ 65 mm (66 mm) reduction in IsoGSM (GPCP) precipitation amount, which accounts for ~ 14% (16%) departure (Δ) from the long-term mean in simulated (observed) precipitation amount.

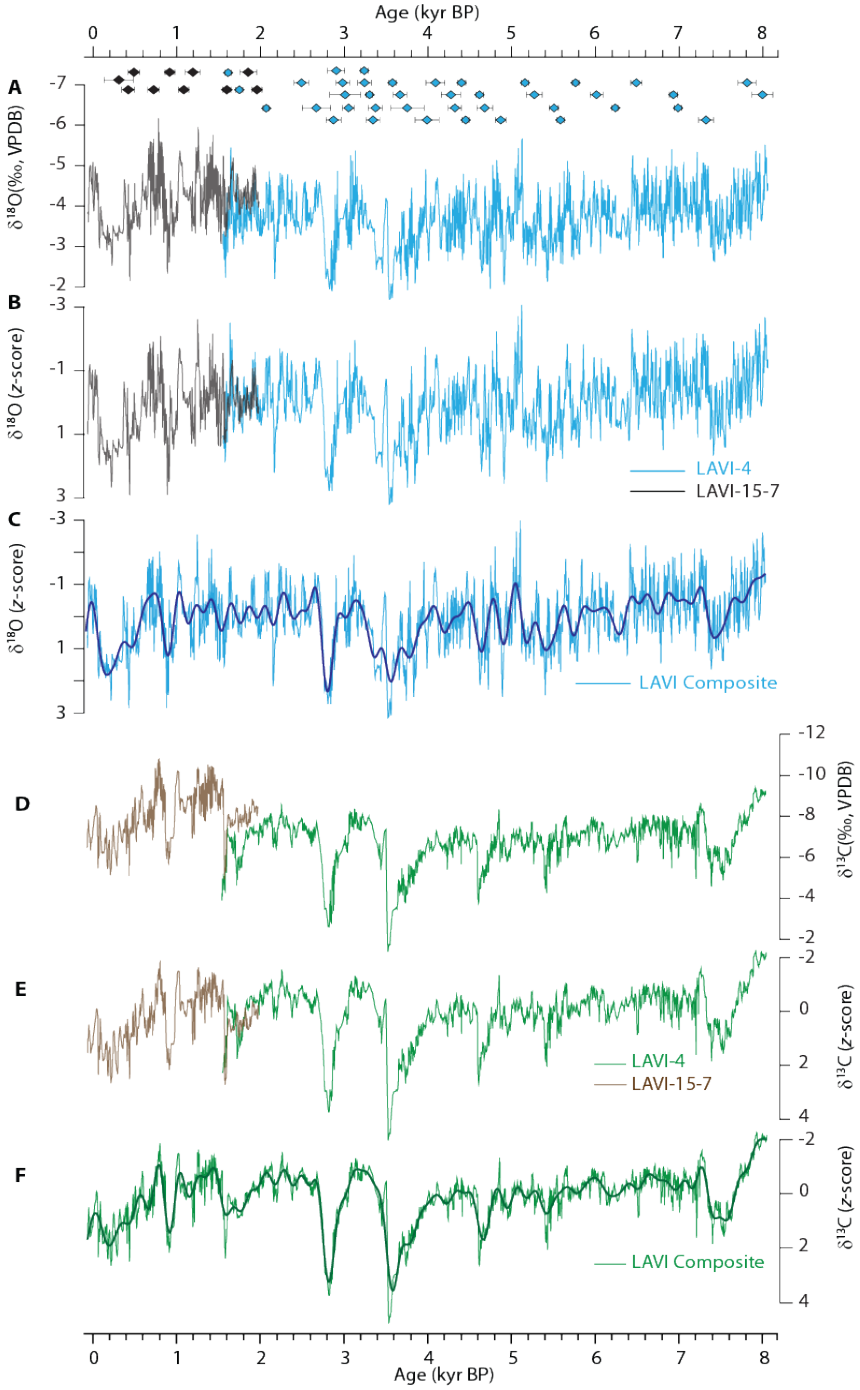

Fig. S6. Raw and composite speleothem records from Rodrigues. (**A**) $\delta^{18}O$ profiles (raw, un-interpolated data) of LAVI-4 (blue) and LAVI-15-7 (black) with ^{230}Th dates and 2σ error bars (color-coded by sample). (**B**) *z*-score transformed and 5 yr interpolated $\delta^{18}O$ profiles of LAVI-4 (blue) and LAVI-15-7 (black). The correlation coefficient between two records for the overlapping part is 0.48. (**C**) Composite $\delta^{18}O$ records of LAVI-15-7 and LAVI- 4 (LAVI composite) and overlapped with a low-pass Butterworth filter (sixth order with a zero-phase lag, thick line) to highlight the multi-centennial variability. (**D-F**) Same as **A-C**, but for $\delta^{13}C$. The correlation coefficient between two records for the overlapping part is 0.23.

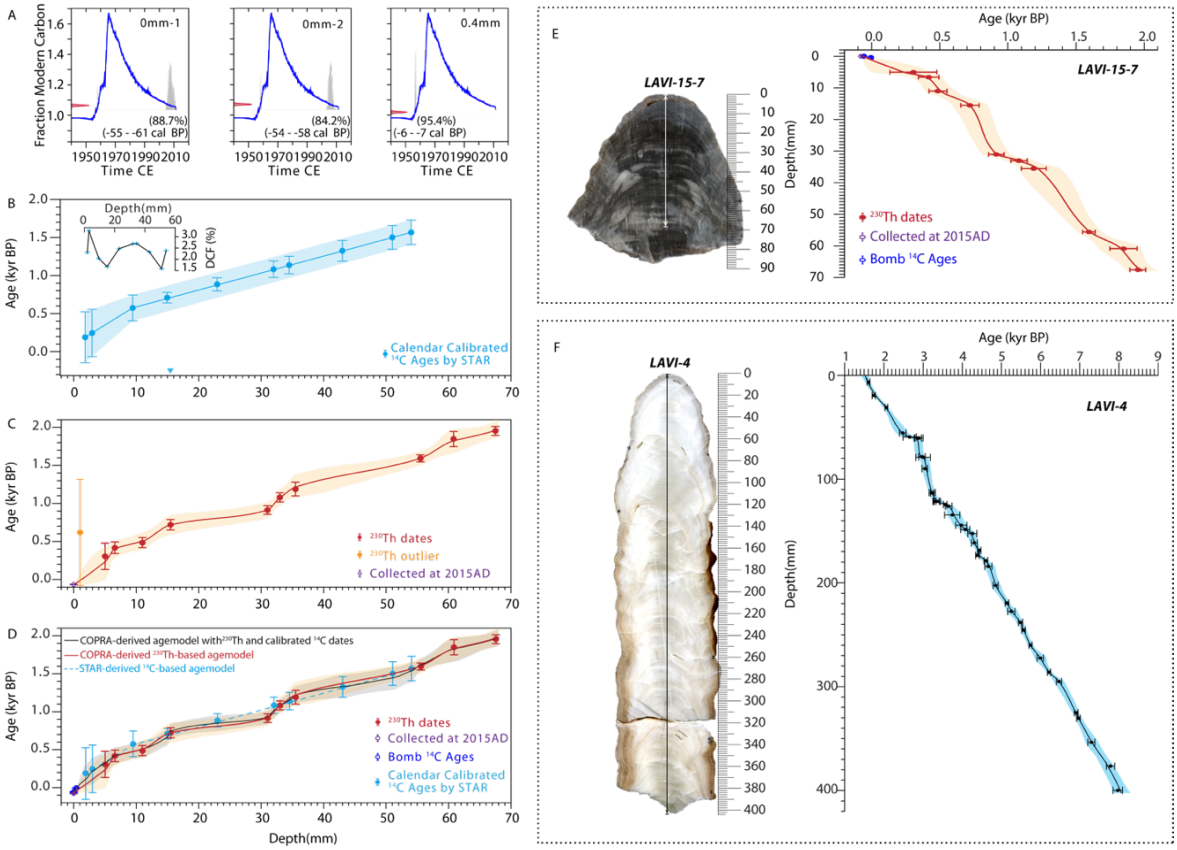

Fig. S7. Age models of Rodrigues speleothem LAVI-15-7 and LAVI-4. (**A**) Calibrated radiocarbon ages of two subsamples (wafers) extracted from the top (left and middle panels) and one powder subsample from ~0.4 mm distance from the top (right panel). The calibration is based on monthly atmospheric ^{14}C curves of the 'bomb peak' (blue) for Southern Hemisphere zone 1-2 (between ~10°S and 90°S over the Indian Ocean section) between 1950 and March 2011 (*52*). (**B**) Calibrated radiocarbon ages and corresponding error bars (2σ analytical error) (blue) and 95% confidence interval (shaded) (*55*) (Materials and Methods). Dead carbon fraction (DCF) deduced from STAR is shown in the inset. (**C**) ^{230}Th-based LAVI-15-7 age model (red) and 95% confidence interval (shaded) derived from COPRA (*41*). (**D**) Age- model comparison showing (1) STAR-derived radiocarbon-based age model (blue dashed line and blue dots, same as **B**), (2) COPRA-derived ^{230}Th-based age model (red solid line and dots, same as **C**) with 95% confidence interval (shaded), (3) COPRA-derived age model (black solid line) using both ^{230}Th dates (10 dates) and calibrated ^{14}C dates (13 dates) along with 95% confidence interval band (gray). (**E**) Scan of LAVI-15-7 in the left panel and COPRA-derived age model (red) with 95% confidence interval (shaded) was selected as the final age model. Double white arrow marks the portion of LAVI-15-7 used in this study. Bomb ^{14}C ages (blue) and the estimated age of the top of the sample, assuming the speleothem was growing when it was collected in 2015 AD (-65 yr BP), are in good agreement. (**F**) Same as **E** but for LAVI-4. Error bars on ^{230}Th dates represent 2σ analytical errors. Double black arrow marks the portion of LAVI-4 used in this study. The true color of speleothem LAVI-15-7 is similar to LAVI-4, which is white. Photo credit: Hanying Li, Xi'an Jiaotong University, Xi'an, China.

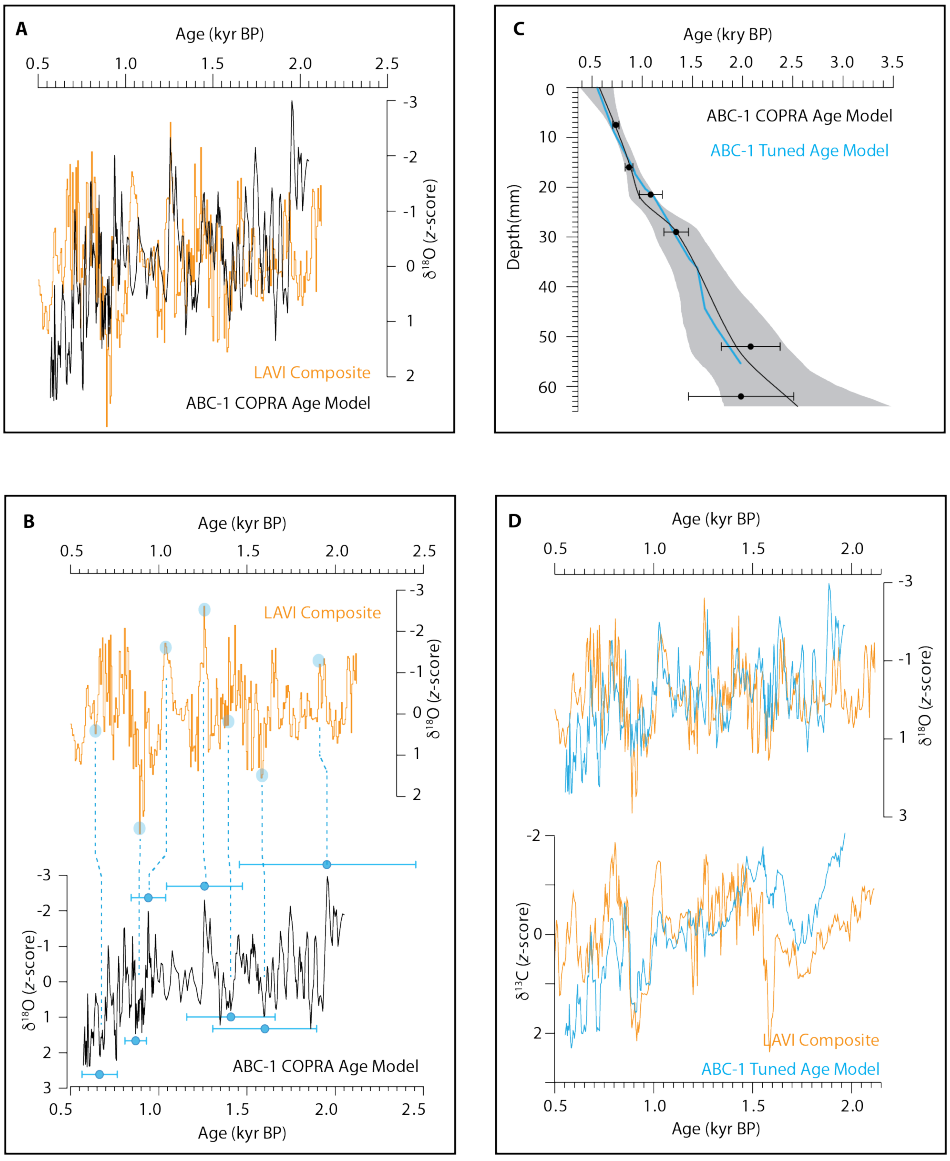

Fig. S8. Age model of a Madagascar speleothem ABC-1. (**A**) Comparison between *z*-score transformed $\delta^{18}O$ profiles between LAVI composite (orange) and ABC-1 (black) on their own COPRA-derived age models. (**B**) Tuned age model of ABC-1 by wiggle-matched process. Comparison between COPRA-derived $\delta^{18}O$ profiles of LAVI composite and ABC-1. The COPRA-derived $\delta^{18}O$ profiles of LAVI composite (upper panel) and ABC-1 (bottom panel) show similar variability with some mismatch due to large age uncertainties of ABC-1. For better age control, the LAVI composite $\delta^{18}O$ record was used to calibrate the age model of ABC-1 within its dating error. Ages at seven tie points of the ABC-1 $\delta^{18}O$ profile (dark blue dots) were transferred from the LAVI composite $\delta^{18}O$ record (light blue dots and dashed lines). The difference between tuned (dark blue) and target (light blue) points is within the 2σ error. (**C**) Age model comparison between tuned (blue) and COPRA-derived age model (black). ^{230}Th dates with 2σ error bars (black) and 95% confidence interval (shaded grey) of COPRA age model are shown. (**D**) Comparison between $\delta^{18}O$ and $\delta^{13}C$ profiles of ABC-1 (blue) with tuned age model and LAVI composite (orange) are shown in the upper and bottom panels, respectively.

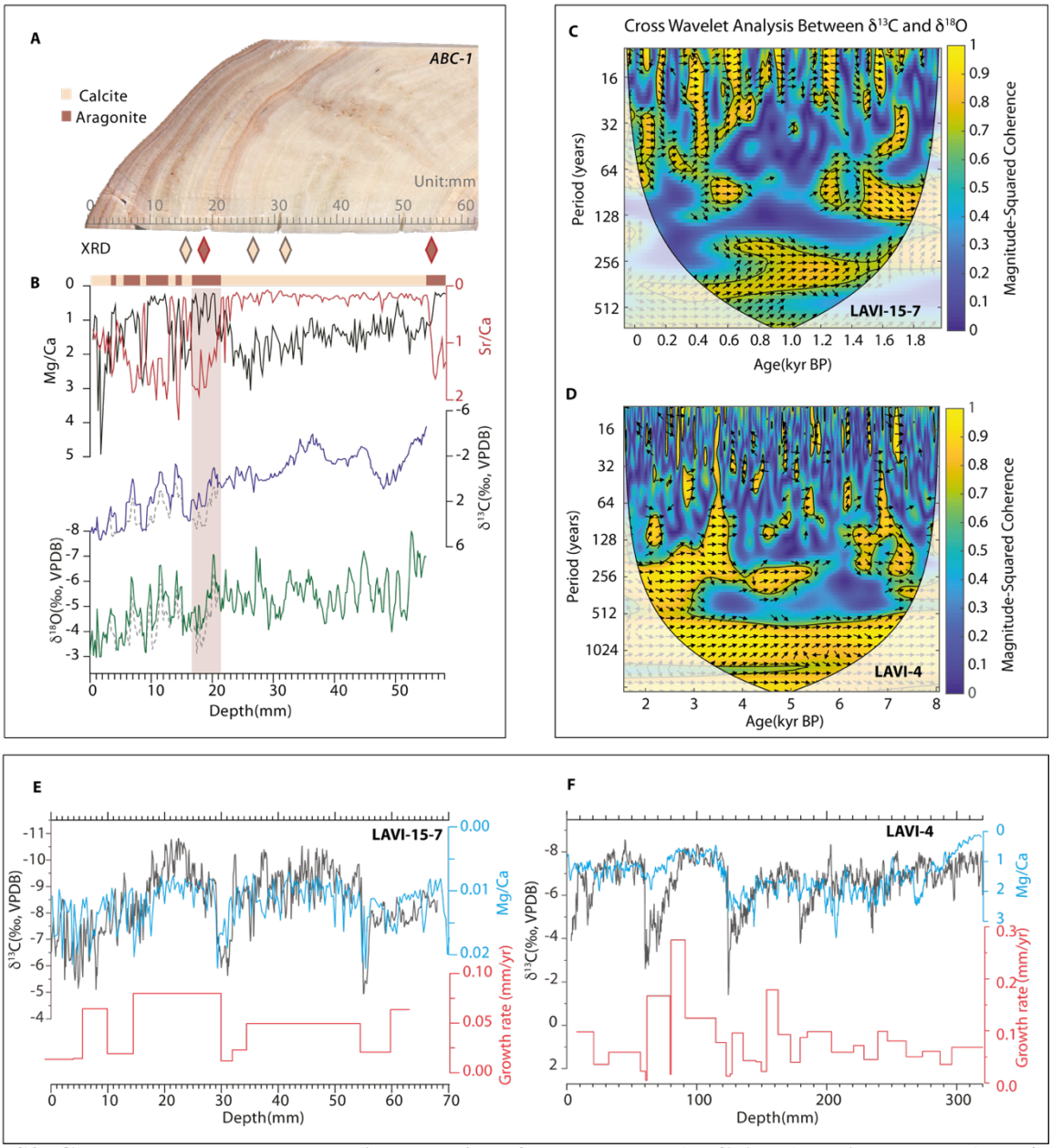

Fig. S9. Growth rates and geochemical proxies of speleothems ABC-1, LAVI-15-7 and LAVI-4. (**A**) High-resolution scan of a polished section of ABC-1. (**B**) XRD measurements of five discrete subsamples showing aragonite (dark brown) and calcite (light brown) layers(diamonds) (Materials and Methods). Mg/Ca (black) and Sr/Ca (brown) trace-element ratio profiles. Calcite (aragonite) layers are identified by higher (lower) Mg/Ca and lower (higher) Sr/Ca indicated by light brown (dark brown) horizontal bars. Stable isotope values of aragonite portions in ABC-1 were corrected to calcite by -1.7‰ for $\delta^{13}C$ and -0.75‰ for $\delta^{18}O$. Corrected $\delta^{13}C$ and $\delta^{18}O$ data are shown by solid purple and green lines, respectively, and raw data (dashed lines). A prominent positive excursion and mineralogy transition are marked by a vertical light brown bar. Photo credit: Hanying Li, Xi'an Jiaotong University, Xi'an, China. (**C** and **D)** Cross wavelet analysis between $\delta^{18}O$ and $\delta^{13}C$ for LAVI-15-7 (**C**) and LAVI-4 (**D**). The coherence of relationship with 95% confidence intervals is shown by solid contour lines. The right oriented arrows indicate zero lag between $\delta^{18}O$ and $\delta^{13}C$. (**E)** $\delta^{13}C$ (black), Mg/Ca ratio (blue) and growth rate (red) of LAVI-15-7 with respect to the depth from 68 to 0 mm. (**F**) Same as **E** but for LAVI-4 for 320 to 0 mm depth.

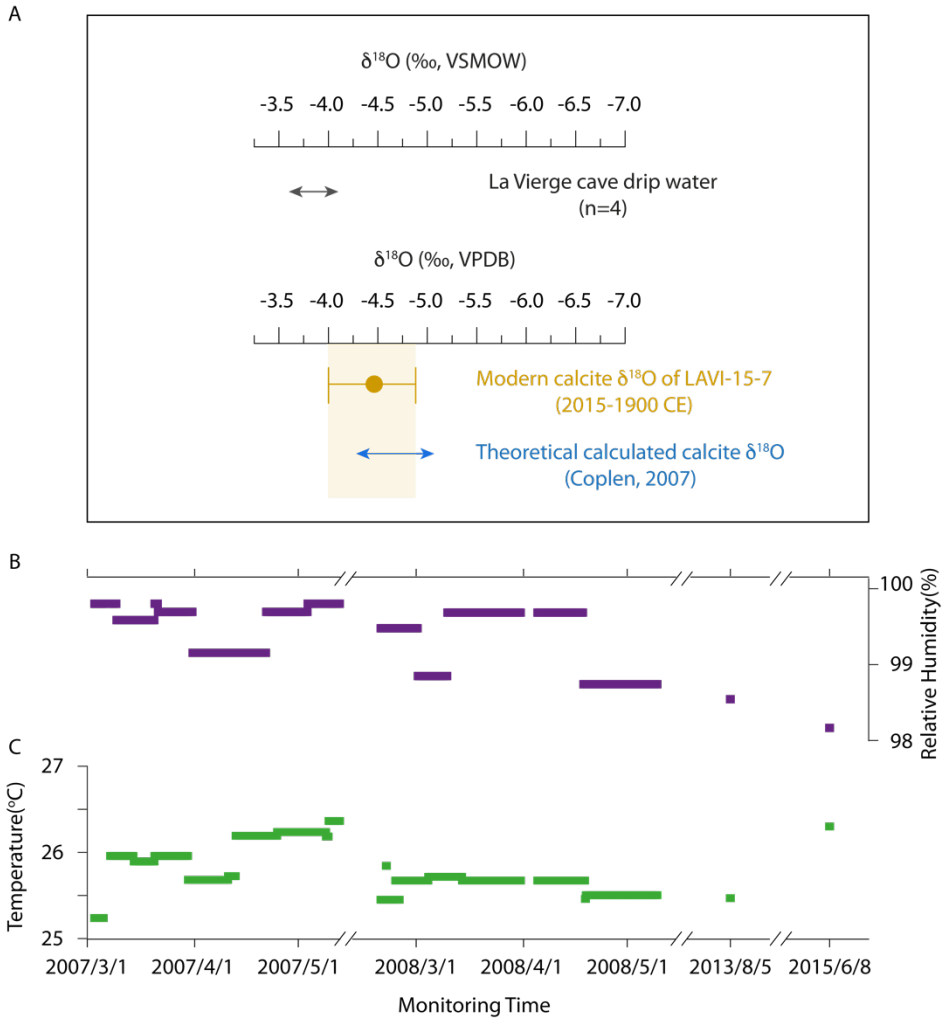

Fig. S10. $\delta^{18}O$ values of drip water, modern calcite and cave monitoring data. (A) The $\delta^{18}O_w$ range from four drip water samples from La Vierge cave (double arrow). Drip water samples were collected between 5th June and 9th June 2015. The yellow circle and associated error bars represent the mean one standard deviation of $\delta^{18}O$ values from the top few mm of LAVI-15-7 corresponding to interval 1900 and 2015 CE. The range of theoretical calcite $\delta^{18}O_c$ values were calculated using fractionation equation (*56*) with measured cave drip water $\delta^{18}O_w$ and monitored cave temperature (25-26.5°C). (**B** and **C**) Continuous relative humidity and temperature measurements (4-hour increment) from La Vierge cave from March to May in 2007 and 2008 and the spot measurements in 2013 and 2015 are shown in purple (**B**) and green (**C**) dots, respectively.